Calcium versus potassium selectivity in a nanopore: the effect of charge inversion at localized pore charges

Hajnalka Fábián[a], Zsófia Sarkadi[a], Mónika Valiskó[a], Dirk Gillespie[b], Dezső Boda[a,*]

[a] *Center for Natural Sciences, University of Pannonia, Egyetem u. 10, Veszprém, 8200, Hungary*
[b] *Department of Physiology and Biophysics, Rush University Medical Center, Chicago, Illinois 60612, USA*

Abstract

The Anomalous Mole Fraction Effect (AMFE) in negatively charged pores has been considered as a signature of Ca^{2+} vs. monovalent ion (K^+, in this study) selectivity. Increasing the mole fraction of $CaCl_2$ in the $KCl/CaCl_2$ mixture, the total conductance first declines as Ca^{2+} ions replace K^+ ions inside the pore, then it increases as Ca^{2+} becomes the main charge carrier. While the AMFE was first pointed out in calcium selective ion channels, in a previous study (Gillespie et al., Biophys. J. 95 (2008) 609–619.) we showed that it is also present in synthetic nanopores. Here we use the Local Equilibrium Monte Carlo method coupled to the Nernst-Planck transport equation to study a simple model of a finite nanopore in a membrane with ions being explicitly modeled as charged hard spheres and water as an implicit continuum. The novel component of the model is the treatment of the pore charges that are present in localized COO^- groups on the wall of the nanopore. Therefore, we study the effect of localizing the pore charges instead of smearing them as a continuous surface charge. Localized charges profoundly influence Ca^{2+} vs. K^+ selectivity because they enhance charge inversion at the pore wall. Ca^{2+} ions overcharge the pore wall at which the K^+ ions have a disadvantage in the K^+ vs. Ca^{2+} competition because the overcharged pore wall does not attract them so strongly.

1. Introduction

Doug Henderson was a great master of our generation, and I (D. Boda) had the honor to be his Padawan. This paper is dedicated to his memory. It was a decisive step in my career when Doug approached me to do Monte Carlo (MC) simulations for certain colleagues named Wolfgang Nonner and Bob Eisenberg (the complete story is found in Bob's paper in this issue [1]). The question was whether we can figure out a simple model that can reproduce an interesting biophysical phenomenon called the Anomalous Mole Fraction Effect (AMFE).

It was presented to us for the L-type calcium channel, which is a very important ion channel in the membrane of muscle cells and neurons and is responsible for letting Ca^{2+} into the cell when the action potential arrives and opens the channel. Those calcium ions do other important things in the cell, but for now it is enough to say that this L-type calcium channel is a pore that is highly selective for Ca^{2+} against monovalent ions, Na^+ and K^+, for example. In experiments, when Almers and McCleskey gradually added $CaCl_2$ to a background of 32 mM NaCl, as little as 10^{-6} M Ca^{2+} is enough to block the Na^+ current (black solid curve with circles in Fig. 1). [2, 3] The curve has a minimum where Na^+ does not carry current because it is squeezed out of the pore, but Ca^{2+} does not carry current either because it is present in the bulk in small concentration. [4–8]

Wolfgang and Bob realized that certain assumptions of the excess chemical potentials produced a "rainbow" of anomalous phenomena. [11]. Later, they used the bulk Mean Spherical Approximation [12] to quantify ionic correlations expressed by the excess chemical potential. Using a bulk theory made Doug jump up at BYU, stating that you cannot use a bulk theory in strongly inhomogeneous circumstances.

That led to that historical hiking of Doug with Wolfgang and Bob in Utah and to a series of papers [4–8, 13–17] in which we used a model that was an inhomogeneous version of the original model of Wolfgang and Bob. It had been named charge-space competition (CSC) mechanism and states that Ca^{2+} has an advantage over Na^+ in the very narrow and crowded selectivity filter of the channel because it provides twice the charge to neutralize the negative stuctural charges of the

*Author to whom correspondence should be addressed.
E-mail address: boda@almos.uni-pannon.hu

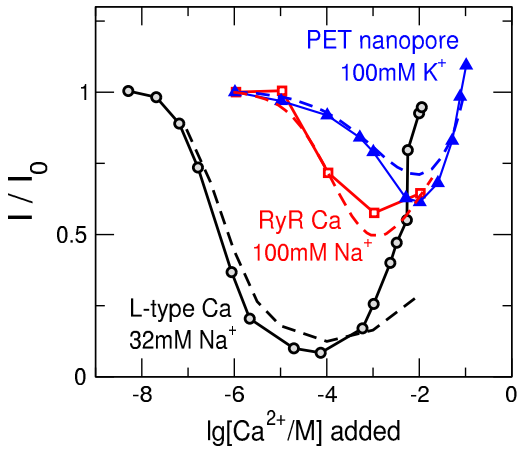

Figure 1: The AMFE experiments for different nanopores: Ca^{2+} is added to a fixed background of monovalent salt. The normalized (I_0 is the current in the absence of Ca^{2+}) current is plotted as a function of the 10-based logarithm of the concentration of the added Ca^{2+} measured in M. In the case of the L-type calcium channel (black), $CaCl_2$ is added to a background of 32 mM NaCl [2, 3]. The black dashed line is the result of previous MC simulations [4]. In the case of the Ryanodine Receptor (RyR) calcium channel (red), $CaCl_2$ is added to a background of 100 mM NaCl. The red dashed line is the result of DFT calculations of Gillespie. [9] In the case of a synthetic PET (Polyethylene terephthalate) nanopore (blue), $CaCl_2$ is added to a background of 100 mM KCl. The blue dashed line is the result of previous MC simulations. [10]

selectivity filter (four COO^- groups altogether in a very small volume) while occupying about the same space. This is basically a competition of energetic (electrostatic attraction) and entropic (hard-sphere exclusion) effects.

Before our CSC model, this high selectivity was attributed to a picture of ions diffusing through the pore in single file. This model received a serious wound when Michael Fill performed similar AMFE measurements for the Ryanodine Receptor (RyR) [9, 18], following earlier AMFE experiments in mixtures of monovalent ions by Gerhard Meissner [19]. Because the RyR selectivity filter was known to be much wider than that of the L-type calcium channel, single filing was unlikely. The calcium AMFE was found in this channel too (red solid curve with squares in Fig. 1) and the density functional theoretical (DFT) results of Dirk Gillespie based on the CSC approach (red dashed line in Fig. 1) nicely reproduced the experimental data (actually, predicted them, because the calculations preceded the measurements). [9, 18, 19] The RyR channel is less selective for Ca^{2+} over Na^+, which is manifested in that the I/I_0 curve starts declining at larger Ca^{2+} concentration and that the minimum is less deep.

The pervasive idea that single-filing was the only cause of AMFE was finally killed when the AMFE was found in synthetic nanopores whose diameter is much larger than that of ion channels. [10] The pores used in the experiments of Zuzanna Siwy were biconical, with a "bottleneck" in the middle with diameters about 5 nm. Single-filing is out of question in such wide pores. A curve for a $CaCl_2$ added to 100 mM KCl experiment is shown in Fig. 1 with blue solid line and triangles.

In our 2008 papers on the AMFE, we reported a simple theoretical framework that is based on dividing the nanopore into slices considered as resistors connected in series. [4, 10] The electrical conductance of each ionic species in a slice was assumed to be proportional to its average ionic concentration in the slice. The average concentration was computed from the radial concentration profiles obtained from equilibrium Grand Canonical Monte Carlo (GCMC) simulations performed for the slices. These simulations for the slices were independent, with each performed for an infinitely long nanopore (periodic boundary condition in the axial dimension) of a given diameter. The negative surface charge ($\sigma = -1\ e/\mathrm{nm}^2$) was smeared on the wall of the pore as a collection of fractional point charges on a fine grid that reproduced the prescribed surface charge density, σ. The adjustable parameter of that model was the effective diffusion coefficients of the ions. This was a concentration dependent parameter. The result of the calculation is shown in Fig. 1 with blue dashed line.

In this paper we return to this problem for several reasons. (1) Now we have a non-equilibrium simulation method that combines the Nernst-Planck (NP) equation with GCMC simulations and provides ionic fluxes that are the natural outputs of experiments. This method had been developed in 2012 [20] and was not available at the time of our previous simulations (2008). (2) Here, we have a finite pore embedded in a membrane that makes it possible to study axial effects. (3) We find it important to model the surface charges as localized at given positions on the pore wall instead of continuously smeared over the surface. [21] Because the surface charge is present in discrete COO^- groups on the surface of the PET nanopore, this is a more realistic model, and, as we will see, gives better results.

2. Model and method

We use a reduced model, by which we mean that the number of degrees of freedom of the system is reduced, i.e., some of the degrees of freedom

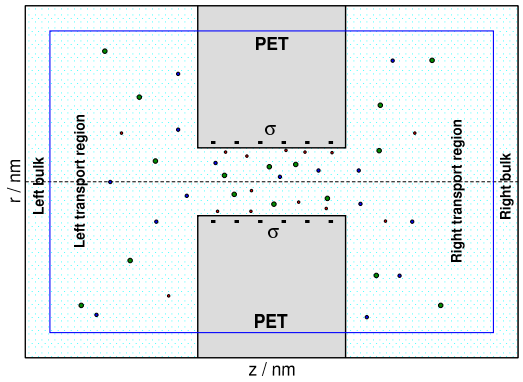

Figure 2: Schematic drawing of the simulation cell.

are not treated explicitly, but are taken into account in some approximate way. The most important such reduction is to consider water molecules implicitly as a medium rather than explicitly as molecules. Implicit water interacts with ions in different ways (dielectric screening and friction) represented by response functions (dielectric constant, ϵ, and diffusion coefficient, $D_i(\mathbf{r})$). The criterion for building a good reduced model is to explicitly consider the important degrees of freedom, while implicitly considering the less important ones, but in a way that is consistent with the physics of nanopore current conduction. [21]

Using a reduced model instead of a more detailed one can be advantageous for several reasons. It is computationally cheaper that is an important issue when we need to perform simulations for a large number of state points at various conditions as it is the case in this study. Furthermore, efficiently sampling of milimolar and lower concentrations in all-atom molecular dynamics (MD) simulations is extremely difficult. Indeed, explicit-water MD simulations for selectivity in electrolyte mixtures are relatively scarce in the literature [22–24]. Finally, starting with simple models and making them more complex gradually is a useful engineering approach that we also apply in this work.

2.1. Model of the nanopore

The model is composed of two parts: a cylindrical nanopore embedded in a membrane and two bulk phases on either side of the membrane. A schematic of the simulation cell is shown in Fig. 2. The figure is rotated around the z-axis to obtain a three-dimensional model with the nanopore (with length, H, and radius, R) in the center. The walls of the pore and the membrane (the thick black line bordering the grey area) are rigid, so that ion overlap with the walls is forbidden.

The space containing the electrolyte solution (light blue area in Fig. 2) can be further divided into two parts: the transport regions and the equilibrium bulk phases (constant chemical potentials). In the transport regions, the chemical potential is not constant, therefore, a transport process (electrodiffusion) takes place. We impose boundary conditions at the interface separating the two parts of the space (blue line in the figure), as this is the interface that bounds our domain of solution.

Table 1: Pauling diameters and bulk-phase diffusion constants of ions.

Ion	d_i / nm	D_i^{bulk} / $\mathrm{m^2 s^{-1}}$
K^+	0.266	1.96×10^{-9}
Ca^{2+}	0.198	0.792×10^{-9}
Cl^-	0.362	2.032×10^{-9}

One of these boundary conditions is the electrostatic (Dirichlet) boundary condition imposed on the boundary of the solution domain, which allows us to model the electrodes. We create an electrical potential difference (voltage, U) between the two sides of the membrane by setting the left half-cylinder to the prescribed voltage and the right half-cylinder to 0 V.

The ions of the electrolyte are explicitly modelled, i.e., the ions are treated as hard spheres with point charges in their centers (the "primitive" model of electrolytes). The spheres cannot overlap, either with the membrane wall or with each other. The interaction between ions is

$$u(r) = \begin{cases} \infty & \text{for} \quad r < (d_i + d_j)/2 \\ \dfrac{1}{4\pi\epsilon_0\epsilon}\dfrac{q_i q_j}{r} & \text{for} \quad r \geq (d_i + d_j)/2 \end{cases}, \tag{1}$$

where d_i and d_j are the ionic diameters of species i and j, ϵ_0 is the permittivity of vacuum, r is the distance between the centers of the ions, and q_i and q_j are the charges of the ions ($q_i = z_i e$, where z_i is the ionic valence and e is the charge of the proton).

The diameters of the ions are twice the Pauling radii. We prefer the Pauling radii to the increased "solvated radii" of the ions in implicit solvent as in many previous studies for ion channels [4–6, 8, 16, 21, 25], nanopores [10, 26, 27], and bulk solutions [28–31]. The effect of the hydration shell on the adsorption of ions at charged surfaces can be taken into account by an adjusted distance of closest approach of the cations to the localized charged groups. This effect will be considered in future studies. Experimental diffusion constants are applied in the bulk phase (D_i^{bulk}, see Table 1).

The pore wall is negatively charged. To be consistent with the experimental situation [10], we use a surface charge density of $\sigma = -1$ e/nm^2 by

Figure 3: A homogeneous (left panel) and a localised (right panel) charge distribution (in blue).

distributing fractional point charges in a grid on the inner wall of the pore such that the sum of the point charges divided by the surface area of the pore wall gives the required charge density. The charges cannot move.

The grid spacing (Δx) is a variable in this study. If, for example, a $\Delta x \approx 0.2$ nm for a pore of length $H = 6$ nm, then 2550 point charges are placed on 30 rings, where the magnitude of the point charges is $-0.0399167\,e$. This fine grid mimics well the uniform and continuous charge distribution used in theories (left side of Fig. 3).

If the Δx parameter is increased, the size of the point charges must be increased to obtain the required -1 e/nm^2. If $\Delta x = 1$ nm, for example, the magnitude of the point charge is $-e$. This is consistent with the experimental setup where the wall charges are localized in COO^- groups (right side of Fig. 3).

The grid is constructed as a series of rings in distance Δx from each other. The distance of charges inside a ring is not necessarily equal to Δx but as close as possible. This allows us to monitor the effect of localized charges in the axial concentration profiles in the form of cation peaks at the rings and/or depletion zones in between.

2.2. NP+LEMC method

The driving force for diffusion is the gradient of the chemical potential in the NP equation:

$$\mathbf{j}_i(\mathbf{r}) = -\frac{1}{kT} D_i(\mathbf{r}) c_i(\mathbf{r}) \nabla \mu_i(\mathbf{r}), \tag{2}$$

where $\mu_i(\mathbf{r})$ varies from place to place. In this equation k is the Boltzmann constant (1.38×10^{-23} J/K), T is the temperature ($T = 298.15$ K), $\mathbf{j}_i(\mathbf{r})$ is the particle current density, $D_i(\mathbf{r})$ is the diffusion coefficient profile, $c_i(\mathbf{r})$ is the concentration profile, and $\mu_i(\mathbf{r})$ is the chemical potential profile.

The diffusion constant profile is constructed as a step function, where its value for a given ion is a constant outside the pore (D_i^{bulk}, see Table 1) and a different constant (D_i^{pore}) inside the pore:

$$D_i(z) = \begin{cases} D_i^{\mathrm{pore}} & \text{for} \quad |z| < H/2 \\ D_i^{\mathrm{bulk}} & \text{for} \quad |z| \geq H/2 \end{cases} \tag{3}$$

The value D_i^{pore} is used as a fitting parameter, i.e., its value is fitted so that the calculated conductivity matches the experimental value.

To couple the NP equation with GCMC simulations, Boda and Gillespie introduced the Local Equilibrium Monte Carlo (LEMC) method [20], in which the simulation cell is divided into small volume elements and a local chemical potential is imposed in each one. The simulation then proceeds as a standard GCMC simulation except that a particular volume element is assumed to be in equilibrium with a bath whose chemical potential is equal to the chemical potential of the given volume element. Accordingly, the variables in the acceptance criterion are the chemical potential and volume of the volume element and number of ions in the volume element (the formulas can be found in the original communication [20]).

The LEMC simulation provides the concentration profile, $c_i(\mathbf{r})$, as an output to the the chemical potential profile, $\mu_i(\mathbf{r})$, as an input. The NP equation must be solved together with the LEMC simulation in a self-consistent way such that the continuity equation describing the conservation of mass is also satisfied:

$$\nabla \cdot \mathbf{j}_i(\mathbf{r}) = 0. \tag{4}$$

To do this, an iteration method is used that varies the chemical potential (and thus the concentration and flux) until the continuity equation is satisfied. This iteration method is used to couple the LEMC simulation to the NP transport equation (NP+LEMC method).

The total flux through the cross-section A from the current density determined from Eq. 2 is given by

$$J_i = \int_A \mathbf{j}_i \cdot \mathbf{n}\, \mathrm{d}a \tag{5}$$

where $\mathbf{n}$ is the normal vector perpendicular to the cross section A. This gives the total electric current flowing through the pore,

$$I = \sum_i q_i J_i = \sum_i I_i. \tag{6}$$

The conductivity of the pore is

$$G = \frac{I}{U}, \tag{7}$$

while the conductivity for a given ion can be calculated from

$$G_i = \frac{I_i}{U}. \tag{8}$$

3. Results and Discussion

There are several ways to perform experiments for mixtures of $\mathrm{CaCl_2}$ and KCl. One is the

added-salt experiment depicted in Fig. 1 where $CaCl_2$ is added to a fixed KCl backround gradually. The other one is the actual mole-fraction experiment where the total concentration $c_{tot} = [CaCl_2] + [KCl]$ is kept fixed (another version is when the total ionic strength is kept fixed).

The two experiments are practically the same for low Ca^{2+} concentrations, but they become different when $[CaCl_2] \sim [KCl]$. In this work, we perform simulations for the second kind of experiment because experimental data are available mostly for this setup in Ref. [10]. The total concentration is $c_{tot} = 100$ mM in this work.

The nanopore in the experiment [10] was a biconical pore fabricated in a 12 μm thick PET membrane by the track-etching technique from the two sides. The radius of the pore in the middle at bottleneck was 2.7 nm, while it was 79 nm at the entrances of the pore. This results in a 0.73° cone angle. The narrow central section of the nanopore, therefore, is long enough to dominate the selectivity of the pore. As a consequence, we use a finite cylindrical nanopore in this study with a fixed radius of $R = 2.7$ nm.

The length of the real nanopore (12 μm), however, is much larger than the length of our model nanopore (H) that is in the nanometer range. Because the conductance of the pore is inversely proportional to the length of the pore, the conductance of the real nanopore is much smaller than that of the model nanopore. In our model, we balance this difference by fitting the diffusion coefficients of the cations in the pore, D_i^{pore}. The length of the pore is a parameter in our model in the range $H = 6 - 18$ nm.

We show the AMFE results as a function of the mole fraction of $CaCl_2$ defined as $\eta = [CaCl_2]/c_{tot}$. At the ends of the mole fraction scale, for the values $\eta = 0$ and $\eta = 1$ we have pure KCl and $CaCl_2$ solutions, respectively. Our strategy is that we fit $D_{K^+}^{pore}$ and $D_{Ca^{2+}}^{pore}$ at the ends ($\eta = 0$ and $\eta = 1$); we calibrate our model to those points. We will validate our model for the mole fraction values in between: $0 < \eta < 1$.

3.1. Fitting the diffusion coefficients in the pore

The details are shown in Fig. 4. Because the bulk diffusion constants are fixed at the experimental values (Table 1), we use ratios of the values in the pore and the bulk as a variable: D_i^{pore}/D_i^{bulk}. It is seen that for this short ($H = 6$ nm) model pore, the D_i^{pore} values need to be reduced $\sim 2-3$ orders of magnitude compared to the bulk values to achieve the experimental conductance. This is in accordance with the difference in the lengths of the real and the model pore: 12 μm vs. 6 nm.

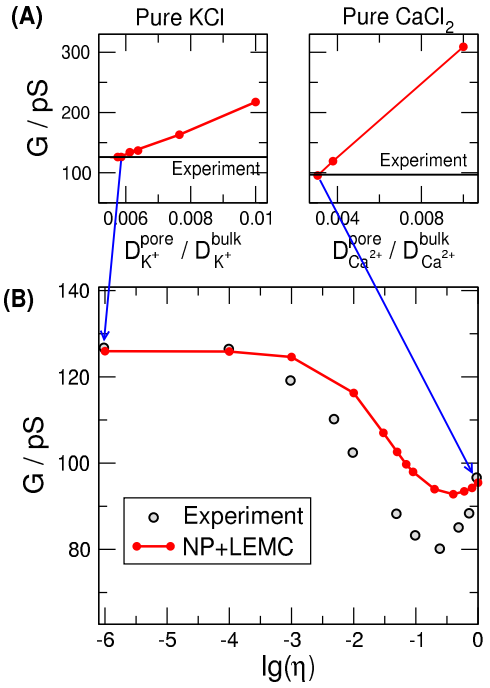

Figure 4: (A) Total conductance as a function of the relative cation diffusion constants, $D_{K^+}^{pore}/D_{K^+}^{bulk}$ and $D_{Ca^{2+}}^{pore}/D_{Ca^{2+}}^{bulk}$ for pure electrolytes. The left figure is for KCl, the right for $CaCl_2$. The black lines show the targeted experimental conductance values. (B) Total conductance as a function of the 10-based logarithm of the mole fraction of Ca^{2+}, $\lg(\eta)$. The black symbols are experimental data, while the red solid line shows the results calculated by the NP+LEMC method using the diffusion coefficients fitted at the endpoints. The system parameters are $H = 6$ nm, $R = 2.7$ nm, $U = 100$ mV, and $\Delta x = 0.2$ nm. The ionic diameters and the bulk diffusion constants, D_i^{bulk}, are found in Table 1.

Because there are two endpoints, we can fit the D_i^{pore} values of the cations. There is, however, a third species, the anion, Cl^-. Instead of choosing a third reference point for fitting, we fix the $D_{Cl^-}^{pore}/D_{Cl^-}^{bulk}$ ratio to that of Ca^{2+}. The effect of this choice will be discussed in Section 3.5.

The procedure is the following. First, we perform simulations for the pure $CaCl_2$ ($\eta = 1$) case and change the diffusion constants of Ca^{2+} and Cl^- together so that $D_{Cl^-}^{pore}/D_{Cl^-}^{bulk} = D_{Ca^{2+}}^{pore}/D_{Ca^{2+}}^{bulk}$. From fitting to experimental conductance values, we obtain this ratio, and, consequently, the $D_{Ca^{2+}}^{pore}$ and $D_{Cl^-}^{pore}$ values. Then, we fix $D_{Cl^-}^{pore}$ and change only $D_{K^+}^{pore}$ in the pure KCl simulations.

3.2. The effect of voltage

The result shown in Fig. 4B is for to a large voltage ($U = 100$ mV), a short pore ($H = 6$ nm), and a fine grid for the surface charge ($\Delta x = 0.2$ nm). The agreement with the experimental data is not very good, therefore, we change the model

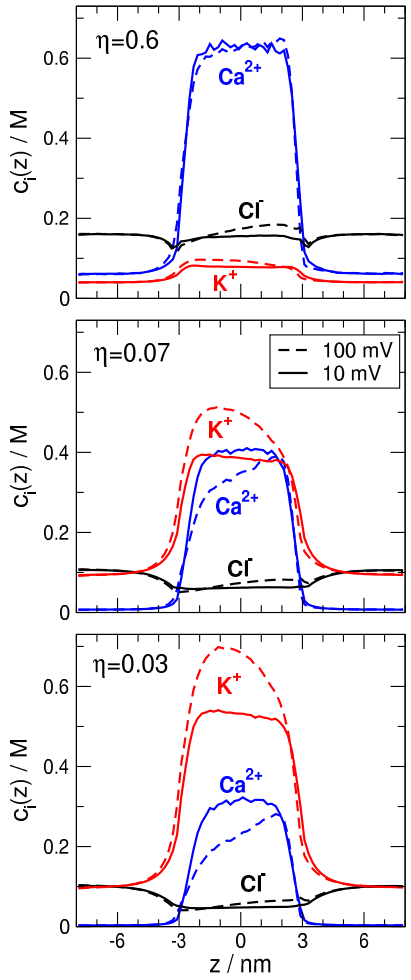

Figure 5: Axial concentration profiles at two different voltages for different Ca^{2+} mole fractions from top to bottom. The pore length is $H = 6$ nm, the radius is $R = 2.7$ nm, the grid width is $\Delta x = 0.2$ nm, while the pore diffusion constants are the values fitted to the pure systems.

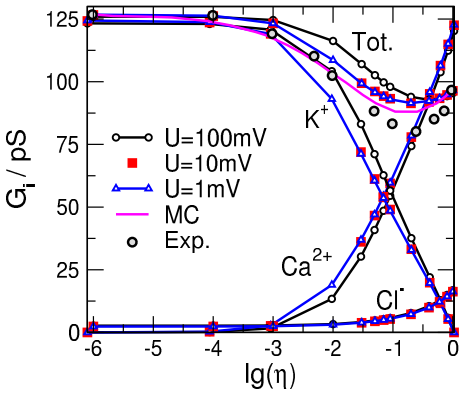

Figure 6: Total conductance and conductances of ions as a functions of the mole fraction of Ca^{2+} at three different voltages. The magenta curve represents the result obtained from the GCMC-based equilibrium calculations [10]. Pore length is $H = 6$ nm, while $\Delta x = 0.2$ nm.

and examine the effect of the above parameters. Let us start with voltage.

Our model pore is short, so the axial effects produced by the charge accumulation at the entrances of the pore on the two sides of the membrane can have a large effect.

These axial effects are clearly shown by the axial concentration profiles in Fig. 5. The concentration profiles are computed as

$$c_i(z) = \frac{1}{A(z)} \int_{A(z)} c_i(\mathbf{r}) \mathrm{d}a, \qquad (9)$$

namely, they are normalized by the cross sectional area, $A(z)$, at coordinate z. The cross section at the entrance of the pore ($|z| \gtrapprox 3$ nm), however, is much larger than inside the pore ($|z| < 3$ nm). The double layers shown by the figure, therefore, store much more charge than implied by the figure.

The charge stored by the double layer has two components. (1) A symmetric cation excess is induced by the negative pore charge; this screens the pore charge "from outside". (2) Voltage induces a positive double layer on one side of the membrane and a negative one on the other side (polarization). This asymmetric ion distribution is superimposed on the symmetric one produced by the pore charge.

It is the second asymmetric component that makes the concentration profiles asymmetric inside the pore when a voltage is applied. Indeed, a considerable slope is observed in the concentration profiles inside the pore at $U = 100$ mV. This influences the competition of K^+ and Ca^{2+} inside the pore and it does so to the benefit of the monovalent ion.

Therefore, to improve Ca^{2+} vs. K^+ selectivity and to bring the $G(\eta)$ curve closer to the experimental one, voltage should be decreased. We have done the simulations (the D_i^{pore} values have been refitted) for $U = 10$ mV and $U = 1$ mV. Fig. 6 shows the total (Eq. 7) and individual (Eq. 8) conductances as functions of $\lg(\eta)$ for different values of the voltage. A considerable difference can be observed between the $U = 100$ mV and 10 mV cases. The G_{K^+} conductance starts declining and the $G_{Ca^{2+}}$ conductance starts rising at smaller η values in the case of $U = 10$ mV. This results in a total G vs. $\lg(\eta)$ curve more similar to the experimental one: the minimum is deeper and it starts declining at smaller η values. The theory of Gillespie et al. [10] (magenta curve), however, still produces better results.

Fig. 6 also shows that the voltages $U = 10$ mV and 1 mV produce the same result. From now on, therefore, we use $U = 10$ mV because it allows better statistics in the simulations.

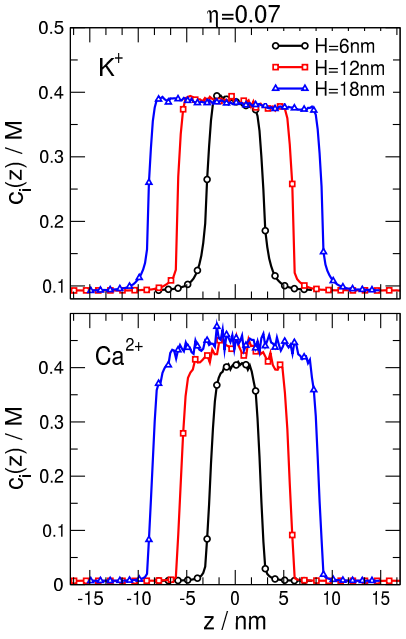

Figure 7: Axial concentration profiles of K^+ (top panel) and Ca^{2+} (bottom panel) for three different pore lengths for a Ca^{2+} mole fraction $\eta = 0.07$. Voltage is $U = 10$ mV, the grid width is $\Delta x = 0.2$ nm.

3.3. The effect of pore length

The length of the real nanopore (~ 12 μm) is large enough so that the effect of the double layers at the pore centers is neglectable. The charges are effectively screened over such a large distance. The model pore, on the other hand is short, so the effect of the symmetric positive double layers is considerable even if the asymmetric component is neglectable at $U = 10$ mV.

Fig. 7 shows the K^+ and Ca^{2+} concentration profiles for a competitive situation ($\eta = 0.07$), where the concentrations of K^+ and Ca^{2+} inside the pore are similar. Decreasing H has a large effect on the Ca^{2+} concentration profiles ($c_{Ca^{2+}}(z)$ decreases as H decreases), while the K^+ profiles are less influenced. This results in a weaker Ca^{2+} vs. K^+ selectivity in shorter pores.

The asymmetry regarding the behavior of the Ca^{2+} and K^+ concentration profiles follows from the asymmetry in the ionic charges. The divalent Ca^{2+} interacts more strongly with the double layers than K^+ does.

The conductances for various pore lengths are shown in Fig. 8. As H is increased, the curves for the total conductance get closer to the one obtained from the slope-conductance theory of Gillespie et al. [10] that can be considered as an infinite pore, zero voltage limit.

The curves for $H = 12$ and 18 nm are quite close to each other, so we have chosen the value $H = 12$ nm to save computer time.

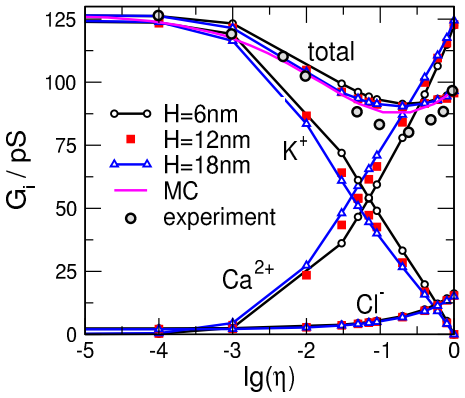

Figure 8: Total conductance and conductances of ions as functions of the mole fraction of Ca^{2+} for three different pore lengths. The magenta curve represents the result obtained from GCMC-based equilibrium calculations [10]. The voltage is $U = 10$ mV, while $\Delta x = 0.2$ nm.

3.4. The effect of the localization of pore charges

The parameters changed so far (U and H) have some effect on selectivity but there is still space for improvement. In the framework of this simple implicit-water model, it is the modeling of the pore charges where we have room for maneuver. The negative charge of the PET membrane is located in discrete deprotonated COO^- groups.

It is interesting that molecular simulations of ionic systems in the implicit-water framework mostly modeled the charges on surfaces as continuous charge distributions since the seminal papers of Torrie and Valleau [32–37]. This had several reasons. (1) It was computationally efficient in the planar geometry to compute the interaction of the ions with the surface charge density if σ was constant. (2) It was mostly the metallic electrode that was in focus. The metallic nature of the electrode can be taken into account with the image charge method in the planar geometry while maintaining the pair-wise additive feature of the interactions. [33, 37] (3) At the beginning, simulations served as gold standard for theories where continuous surface charge distributions are inherent.

If the membrane is made of an insulator, however, the simplification of the continuous surface charge distribution may not be sufficient. Still, the number of studies using localized charges in the implicit-water framework is limited. [38–41] In molecular dynamics simulations, on the other hand, pore charges are naturally modeled as point charges sitting on atoms for explicit-water electrolytes.

Using a continuous surface charge distribution can be a reasonable model for 1:1 electrolytes, but it can have a serious effect if multivalent ions are present. In our previous pa-

per [21], we showed that a selectivity inversion found by the group of Zuzanna Siwy [26] can be reproduced by using localized charges. The experiment showed that a negatively charged nanopore's cation selectivity for a 1:1 electrolyte (KCl) can be turned into anion selectivity if we use a 3:1 electrolyte (cobalt(III) sepulchrate chloride, $CoSepCl_3$). $CaCl_2$ is in between.

The phenomenon was interpreted as a signature of charge inversion. [26] Multivalent ions correlate strongly with the COO^- groups and form relatively long-lived complexes. This results in an overcharging of the pore wall with multivalent cations producing anion excess in the middle of the pore. Also, the multivalent ions are tightly bound to the localized charges, resulting in peaks at the charges and depletion zones in the space between them, see Fig. 9A of Ref. [21]. In that paper we showed that this enhanced charge inversion can be reproduced even in the implicit-water framework where electrostatic forces are strongly screened.

Because charge localization influences monovalent and divalent ions differently, it is reasonable to assume that it has an effect on Ca^{2+} vs. K^+ selectivity.

In the following, we use Δx as the parameter characterizing the "degree of localization". Fig. 9 shows the conductances as functions of Δx for pure KCl (top), pure $CaCl_2$ (middle), and a mixture with $\eta = 0.4$ (bottom). As expected, the conductance of K^+ in pure KCl does not depend on Δx. The conductance of Ca^{2+} in pure $CaCl_2$, on the other hand, exhibits a considerable decrease when Δx rises above 0.75 nm. These results are not surprising and were already seen in Ref. [21].

In the case of the mixture, however, both K^+ and Ca^{2+} conductances decrease with increasing localization. The explanation of this can be deduced from the axial concentration profiles of Fig. 10. For $\Delta x = 0.2$ nm, that practically corresponds to the continuous charge distribution, we observe the smooth concentration profiles (apart from statistical noise, black curves) that we already saw in Figs. 5 and 7. If we increase Δx to 0.75 nm (red curves) or beyond ($\Delta x = 1$ nm, blue curves), peaks appear at the z coordinates that correspond to the rings where the localized charges are placed (right panel of Fig. 3). This is more apparent in the Ca^{2+} concentration profile, while those of Cl^- and K^+ are moderately influenced.

The peaks and the wells (depletion zones) between them are results of the strong correlation between Ca^{2+} ions and the localized charges. This can be characterized by the radial profiles of Ca^{2+} shown in the inset of the bottom panel of

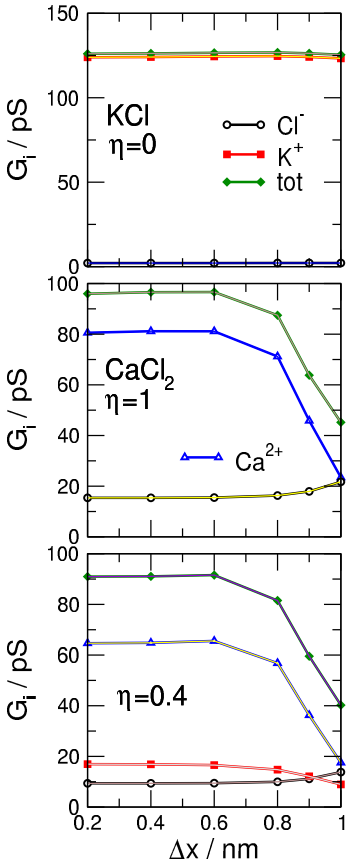

Figure 9: The effect of localized charge distribution on the conduction properties for pure KCl (top panel) and $CaCl_2$ systems (middle panel), as well as for a mixture with $\eta = 0.4$ (bottom panel). Total and ionic conductances are ploted as functions of Δx. The system parameters are $H = 12$ nm and $U = 10$ mV.

Fig. 10. At the z coordinate of a peak the Ca^{2+} concentration (filled blue symbols) is much higher (note the log scale) than at the z coordinate of a well (open blue symbols) in the localized case ($\Delta x = 1$ nm). There is no such difference for the non-localized case ($\Delta x = 0.2$ nm, black symbols).

If we increase Δx even further (1 nm, blue curves), dramatic changes can be seen. The Ca^{2+} concentration profiles exhibit high peaks and depletion zones between them. The depletion zones explain the large reduction of Ca^{2+} conductance observed in Fig. 9.

From the point of view of selectivity, however, it is important that the K^+ concentration decreases inside the pore as Δx increases. The explanation of this behavior is that Ca^{2+} ions overcharge the localized charges and draw in Cl^-, so these charges cannot attract the K^+ ions as efficiently as for small Δx values.

As a consequence, the total conductance decreases with increasing Δx because both Ca^{2+} and K^+ conductances decrease (Fig. 9). The

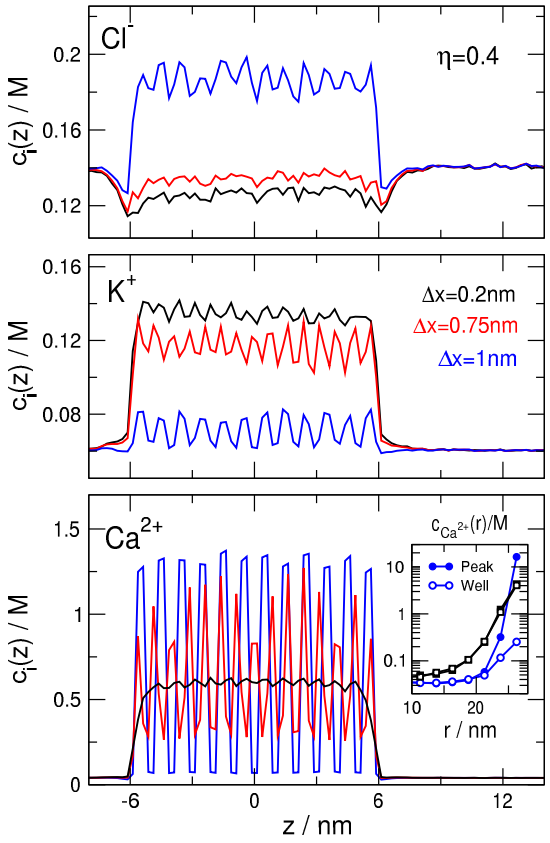

Figure 10: Axial concentration profiles of Cl^- (top), K^+ (middle panel), and Ca^{2+} (bottom panel) for three different pore grid widths, Δx, for $CaCl_2$ mole fraction $\eta = 0.4$. The system parameters are $H = 12$ nm and $U = 10$ mV. The $\Delta x = 1$ case corresponds to the "true" experimental case. The inset in the bottom panel shows radial concentration profiles for Ca^{2+} at z coordinates that correspond to a peak and a well. Black and blue colors refer to $\Delta x = 0.2$ and 1 nm, respectively.

Ca^{2+} conductance decreases because Ca^{2+} ions are tightly bound to the localized charges. The K^+ conductance decreases because there is less K^+ ions in the pore.

The concentration of the Cl^- ions increases with increasing Δx (Fig. 10), but this increase and the associated increase in Cl^- conductance (Fig. 9) is not substantial.

Fig. 11 shows the conductances as functions of $\lg(\eta)$ for different values of Δx. Increasing Δx has an effect on all of the individual species' ionic conductances which together define the total.

Interestingly, Ca^{2+} and Cl^- conductances are correlated. This is shown by the fact that the sum of their conductances is the same for different Δx values (see the inset in the bottom-left panel). As Ca^{2+} conductance decreases with increasing Δx, Cl^- conductance increases. This corresponds to a shift from cation selectivity towards anion selectivity already studied in Ref. [21]. Ca^{2+} ions are bound to the localized charges at large Δx values and overcharge them. Consequently, the pore wall becomes virtually positively charged, which explains the anion leakage.

Since the sum of the conductances of Ca^{2+} and Cl^- are the same for different Δx values, it is the K^+ conductance (top-left panel) that determines the anomalous behavior of the total conductance (top-right panel). As Δx increases, the overcharged pore wall does not attract the K^+ ions so strongly, so a decrease in K^+ concentrations, and, thus, a decrease in K^+ conductance can be observed.

AMFE is characterized by the nonlinear η dependence of the total conductance that, in turn, characterizes Ca^{2+} vs. K^+ selectivity. This selectivity can be quantified either by the η value at which the total conductance starts declining, or the minimum of the curve. In either case, the $\Delta x = 1$ nm localization produces too strong Ca^{2+} vs. K^+ selectivity. This is because the pore charges are placed on the pore wall, so they are in a distance of an ion radius from the ion centers. Consequently, the interaction between the ions and the localized pore charges is overestimated. Other models for pore charges will be considered in later studies.

3.5. Effect of choosing the anion diffusion coefficient in the pore

The $D^{\text{pore}}_{Cl^-}/D^{\text{bulk}}_{Cl^-}$ ratio was fixed to that of Ca^{2+} so far because we wanted focus on K^+ vs. Ca^{2+} and wanted minimize Cl^- leakage. Fitting it to $D^{\text{pore}}_{K^+}/D^{\text{bulk}}_{K^+}$, however, does not make much difference as seen from Table 2. The ratios are in the same ballpark no matter which procedure we choose.

Two conclusions for the fitted diffusion coefficients can be drawn from Table 2. (1) The fitted $D^{\text{pore}}_{K^+}/D^{\text{bulk}}_{K^+}$ ratios are the same independent of the value of Δx. This is because there is no charge inversion in pure KCl, so the pore is K^+ selective over Cl^-. The nature of modeling the pore charge, therefore, does not influence the K^+ diffusion coefficient.

(2) The $D^{\text{pore}}_{Ca^{2+}}/D^{\text{bulk}}_{Ca^{2+}}$ ratio increases as Δx increases even above $D^{\text{pore}}_{K^+}/D^{\text{bulk}}_{K^+}$. This is because larger Δx produces stronger charge inversion and deeper depletion zones for Ca^{2+} (see blue line in the bottom panel of Fig. 10). In the NP equation, the flux is obtained as a product of $D_i(\mathbf{r})$ and a term that depends on local concentration $(c_i(\mathbf{r})\nabla\mu_i(\mathbf{r}))$. These two terms are highly independent of each other. The second term is reduced by the depletion zones so $D_i(\mathbf{r})$ must be increased to reproduce the experimental conductance.

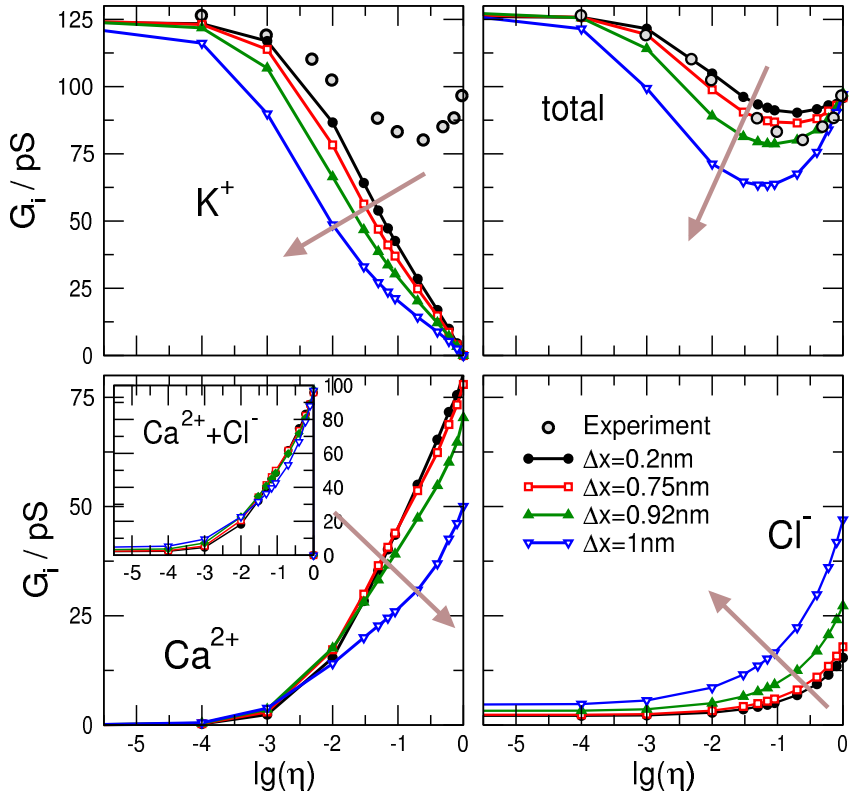

Figure 11: Total conductivity (top-right panel) and conductivities of ions (other panels) as functions of the mole fraction of Ca^{2+} for three different Δx values. The voltage is $U = 10$ mV, while the pore length is $H = 12$ nm. The inset in the bottom-left panel shows the sum of the Ca^{2+} and Cl^- conductivities. Brown arrows show the direction in which Δx increases.

Figure 12 shows these effects in terms of AMFE curves. Charge inversion so strong for $\Delta x = 1$ nm that we obtain similar Cl^- and Ca^{2+} conductances for the $\eta = 1$ endpoint (pure $CaCl_2$). This result is in agreement with the measurements of He et al. [26] and other experimental works. [42–44] He at el. pointed out that cation selectivity is lost for $CaCl_2$ and anion selectivity is obtained for trivalent cations ($CoSepCl_3$).

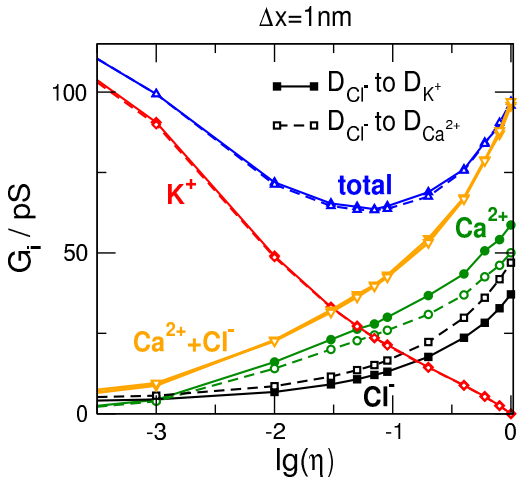

Figure 12: Total conductivity and conductivities of ions as functions of the mole fraction of Ca^{2+} for $\Delta x = 1$ nm for the cases of fitting $D^{\text{pore}}_{Cl^-}/D^{\text{bulk}}_{Cl^-}$ either to $D^{\text{pore}}_{Ca^{2+}}/D^{\text{bulk}}_{Ca^{2+}}$, or to $D^{\text{pore}}_{K^+}/D_{K^+}$. The voltage is $U = 10$ mV, while the pore length is $H = 12$ nm.

Figure 12 shows that the choice of Cl^- diffusion coefficient does not influence the final result for the total conductance because it does not influence the behavior of either G_{K^+}, or $G_{Ca^{2+}} + G_{Cl^-}$. It determines, however, how Ca^{2+} and Cl^- share the $G_{Ca^{2+}} + G_{Cl^-}$ conductance.

4. Summary

In this work, we developed a nanopore model that was able to reproduce the anomalous experimental behavior of the conductance vs. Ca^{2+} mole fraction curve. Because the experimental PET nanopore is long, it was not a surprise that using large pore length and small voltage is advantageous because the axial effects of the access regions at the entrances of the pore are minimized.

This work steps beyond the model of Gillespie et al. [10] (1) by using a non-equilibrium simulation method (NP+LEMC) to estimate the ionic currents and (2) by using localized charges on the

Table 2: Diffusion constants for simulations when $D^{\text{pore}}_{\text{Cl}^-}/D^{\text{bulk}}_{\text{Cl}^-}$ is bound either to $D^{\text{pore}}_{\text{Ca}^{2+}}/D^{\text{bulk}}_{\text{Ca}^{2+}}$, or to $D^{\text{pore}}_{\text{K}^+}/D^{\text{bulk}}_{\text{K}^+}$ for $\Delta x = 0.923$ nm and $\Delta x = 1$ nm. The units of diffusion constants are m^2/s.

	$D^{\text{pore}}_{\text{Cl}^-}/D^{\text{bulk}}_{\text{Cl}^-}$ is bound to $D^{\text{pore}}_{\text{Ca}^{2+}}/D^{\text{bulk}}_{\text{Ca}^{2+}}$		$D^{\text{pore}}_{\text{Cl}^-}/D^{\text{bulk}}_{\text{Cl}^-}$ is bound to $D^{\text{pore}}_{\text{K}^+}/D^{\text{bulk}}_{\text{K}^+}$	
	$\Delta x = 0.923$ nm	$\Delta x = 1$ nm	$\Delta x = 0.923$ nm	$\Delta x = 1$ nm
$D^{\text{bulk}}_{\text{K}^+}/10^{-9}$	1.96			
$D^{\text{pore}}_{\text{K}^+}/10^{-9}$	0.0197	0.0195	0.0195	0.0197
$D^{\text{pore}}_{\text{K}^+}/D^{\text{bulk}}_{\text{K}^+}$	0.01	0.01	0.01	0.01
$D^{\text{bulk}}_{\text{Ca}^{2+}}/10^{-9}$	0.792			
$D^{\text{pore}}_{\text{Ca}^{2+}}/10^{-9}$	0.00711	0.0101	0.00697	0.0118
$D^{\text{pore}}_{\text{Ca}^{2+}}/D^{\text{bulk}}_{\text{Ca}^{2+}}$	0.00898	0.0128	0.0088	0.0149
$D^{\text{bulk}}_{\text{Cl}^-}/10^{-9}$	2.032			
$D^{\text{pore}}_{\text{Cl}^-}/10^{-9}$	0.0182	0.0259	0.0203	0.0204
$D^{\text{pore}}_{\text{Cl}^-}/D^{\text{bulk}}_{\text{Cl}^-}$	0.00898	0.0128	0.01	0.01

pore wall. Using localized charges was a decisive step in better reproducing the experimental data, because charge inversion is enhanced by the localized charges and K^+ ions have a disadvantage in the K^+ vs. Ca^{2+} competition at the overcharged pore wall.

Acknowledgements

We gratefully acknowledge the financial support of the National Research, Development, and Innovation Office – NKFIH K137720 and the TKP2021-NKTA-21. We are grateful to Tamás Kristóf and Zoltán Ható for inspiring discussions.

[1] R. Eisenberg, Meeting Doug Henderson, J. Mol. Liq. 361 (2022) 119574.

[2] W. Almers, E. W. McCleskey, P. T. Palade, A non-selective cation conductance in frog muscle membrane blocked by micromolar external calcium ions., J. Physiol. 353 (1984) 565–583.

[3] W. Almers, E. W. McCleskey, Non-selective conductance in calcium channels of frog muscle: calcium selectivity in a single-file pore, J. Physiol. 353 (1984) 585–608.

[4] D. Gillespie, D. Boda, The anomalous mole fraction effect in calcium channels: A measure of preferential selectivity, Biophys. J. 95 (2008) 2658–2672.

[5] D. Boda, M. Valiskó, D. Henderson, B. Eisenberg, D. Gillespie, W. Nonner, Ion selectivity in L-type calcium channels by electrostatics and hard-core repulsion, J. Gen. Physiol. 133 (2009) 497–509.

[6] M. Malasics, D. Boda, M. Valiskó, D. Henderson, D. Gillespie, Simulations of calcium channel block by trivalent ions: Gd^{3+} competes with permeant ions for the selectivity filter, Biochim. et Biophys. Acta - Biomembranes 1798 (2010) 2013–2021.

[7] D. Boda, J. Giri, D. Henderson, B. Eisenberg, D. Gillespie, Analyzing the components of the free energy landscape in a calcium selective ion channel by Widom's particle insertion method, J. Chem. Phys. 134 (2011) 055102.

[8] D. Boda, D. Henderson, D. Gillespie, The role of solvation in the binding selectivity of the L-type calcium channel, J. Chem. Phys. 139 (2013) 055103.

[9] D. Gillespie, Energetics of divalent selectivity in a calcium channel: The Ryanodine Receptor case study, Biophys. J. 94 (2008) 1169–1184.

[10] D. Gillespie, D. Boda, Y. He, P. Apel, Z. Siwy, Synthetic nanopores as a test case for ion channel theories: The anomalous mole fraction effect without single filing, Biophys. J. 95 (2008) 609–619.

[11] W. Nonner, D. P. Chen, B. Eisenberg, Anomalous Mole Fraction Effect, Electrostatics, and Binding in Ionic Channels, Biophys. J. 74 (1998) 2327–2334.

[12] W. Nonner, L. Catacuzzeno, B. Eisenberg, Binding and selectivity in L-type calcium channels: A mean spherical approximation., Biophys. J. 79 (2000) 1976–1992.

[13] D. Boda, D. D. Busath, D. Henderson, S. Sokołowski, Monte Carlo simulations of the mechanism for channel selectivity: The competition between volume exclusion and charge neutrality, J. Phys. Chem. B 104 (2000) 8903–8910.

[14] D. Boda, D. Henderson, D. D. Busath, Monte Carlo study of the effect of ion and channel size on the selectivity of a model calcium channel, J. Phys. Chem. B 105 (2001) 11574–11577.

[15] D. Boda, D. Henderson, D. D. Busath, Monte Carlo study of the selectivity of calcium channels: improved geometrical model, Mol. Phys. 100 (2002) 2361–2368.

[16] D. Boda, M. Valiskó, B. Eisenberg, W. Nonner, D. Henderson, D. Gillespie, The effect of protein dielectric coefficient on the ionic selectivity of a calcium channel, J. Chem. Phys. 125 (2006) 034901.

[17] D. Boda, M. Valiskó, B. Eisenberg, W. Nonner, D. Henderson, D. Gillespie, Combined effect of pore radius and protein dielectric coefficient on the selectivity of a calcium channel, Phys. Rev. Lett. 98 (2007) 168102.

[18] D. Gillespie, J. Giri, M. Fill, Reinterpreting the anomalous mole fraction effect: The Ryanodine receptor case study, Biophys. J. 97 (2009) 2212–2221.

[19] D. Gillespie, L. Xu, Y. Wang, G. Meissner, (De)constructing the Ryanodine Receptor: Modeling Ion Permeation and Selectivity of the Calcium Release Channel, J. Phys. Chem. B 109 (2005) 15598–15610.

[20] D. Boda, D. Gillespie, Steady state electrodiffu-

sion from the Nernst-Planck equation coupled to Local Equilibrium Monte Carlo simulations, J. Chem. Theor. Comput. 8 (2012) 824–829.
[21] D. Boda, M. Valiskó, D. Gillespie, Modeling the device behavior of biological and synthetic nanopores with reduced models, Entropy 22 (2020) 1259.
[22] I. C. Bourg, G. Sposito, Molecular dynamics simulations of the electrical double layer on smectite surfaces contacting concentrated mixed electrolyte (naclcacl2) solutions, J. Colloid Interf. Sci. 360 (2011) 701–715.
[23] M. F. Döpke, J. Lützenkirchen, O. A. Moultos, B. Siboulet, J.-F. Dufrêche, J. T. Padding, R. Hartkamp, Preferential adsorption in mixed electrolytes confined by charged amorphous silica, J. Phys. Chem. C 123 (2019) 16711–16720.
[24] C. Sögaard, K. Kolman, M. Christensson, A. B. Otyakmaz, Z. Abbas, Hofmeister effects in the gelling of silica nanoparticles in mixed salt solutions, Colloids Surf. A: Physicochem. Eng. Asp. 611 (2021) 125872.
[25] D. Boda, in: R. A. Wheeler (Ed.), Ann. Rep. Comp. Chem., volume 10, Elsevier, 2014, pp. 127–163.
[26] Y. He, D. Gillespie, D. Boda, I. Vlassiouk, R. S. Eisenberg, Z. S. Siwy, Tuning transport properties of nanofluidic devices with local charge inversion, JACS 131 (2009) 5194–5202.
[27] M. Valiskó, B. Matejczyk, Z. Ható, T. Kristóf, E. Mádai, D. Fertig, D. Gillespie, D. Boda, Multiscale analysis of the effect of surface charge pattern on a nanopore's rectification and selectivity properties: from all-atom model to poisson-nernst-planck, J. Chem. Phys. 150 (2019) 144703.
[28] J. Vincze, M. Valiskó, D. Boda, The nonmonotonic concentration dependence of the mean activity coefficient of electrolytes is a result of a balance between solvation and ion-ion correlations, J. Chem. Phys. 133 (2010) 154507.
[29] M. Valiskó, D. Boda, The effect of concentration- and temperature-dependent dielectric constant on the activity coefficient of NaCl electrolyte solutions, J. Chem. Phys. 140 (2014) 234508.
[30] M. Valiskó, D. Boda, Unraveling the behavior of the individual ionic activity coefficients on the basis of the balance of ion-ion and ion-water interactions, J. Phys. Chem. B 119 (2015) 1546–1557.
[31] M. Valiskó, D. Boda, Activity coefficients of individual ions in $lacl_3$ from the ii+iw theory, Mol. Phys. 115 (2017) 1245–1252.
[32] G. M. Torrie, J. P. Valleau, Electrical double-layers 1. Monte Carlo study of a uniformly charged surface, J. Chem. Phys. 73 (1980) 5807–5816.
[33] G. M. Torrie, J. P. Valleau, G. N. Patey, Electrical double-layers 2. Monte-Carlo and HNC studies of image effects, J. Chem. Phys. 76 (1982) 4615–4622.
[34] J. P. Valleau, G. M. Torrie, The electrical double-layer 3. Modified Gouy-Chapman theory with unequal ion sizes, J. Chem. Phys. 76 (1982) 4623–4630.
[35] G. M. Torrie, J. P. Valleau, Electrical double-layers 4. Limitations of the Gouy-Chapman theory, J. Phys. Chem. 86 (1982) 3251–3257.
[36] J. P. Valleau, G. M. Torrie, Electrical double-layers 5. Asymmetric ion wall interactions, J. Chem. Phys. 81 (1984) 6291–6295.
[37] G. M. Torrie, J. P. Valleau, C. W. Outhwaite, Electrical double-layers 6. Image effects for divalent ions, J. Chem. Phys. 81 (1984) 6296–6300.
[38] S. Madurga, A. Martín-Molina, E. Vilaseca, F. Mas, M. Quesada-Pérez, Effect of the surface charge discretization on electric double layers: A monte carlo simulation study, J. Chem. Phys. 126 (2007) 234703.
[39] Z. yong Wang, Y. qiang Ma, Monte carlo determination of mixed electrolytes next to a planar dielectric interface with different surface charge distributions, J. Chem. Phys. 131 (2009) 244715.
[40] P.-A. Cazade, R. Hartkamp, B. Coasne, Structure and dynamics of an electrolyte confined in charged nanopores, J. Phys. Chem. C 118 (2014) 5061–5072.
[41] S. Zhou, Effects of discreteness of surface charges on the effective electrostatic interactions, J. Chem. Phys. 140 (2014) 234704.
[42] F. H. J. van der Heyden, D. Stein, K. Besteman, S. G. Lemay, C. Dekker, Charge inversion at high ionic strength studied by streaming currents, Phys. Rev. Lett. 96 (2006).
[43] J. Loessberg-Zahl, K. G. H. Janssen, C. McCallum, D. Gillespie, S. Pennathur, (almost) stationary isotachophoretic concentration boundary in a nanofluidic channel using charge inversion, Anal. Chem. 88 (2016) 6145–6150.
[44] K.-H. Chou, C. McCallum, D. Gillespie, S. Pennathur, An experimental approach to systematically probe charge inversion in nanofluidic channels, Nano Lett. 18 (2018) 1191–1195.